atmosphere

MDPI

Article

Characterisation of Extreme Precipitation Events in the Pyrenees: From the Local to the Synoptic Scale

Marc Lemus-Canovas [1,*], Joan Albert Lopez-Bustins [1], Javier Martín-Vide [1], Amar Halifa-Marin [2], Damián Insua-Costa [3], Joan Martinez-Artigas [1], Laura Trapero [4], Roberto Serrano-Notivoli [5] and José María Cuadrat [6]

1 Climatology Group, Department of Geography, University of Barcelona, c/Montalegre, 6, 08001 Barcelona, Spain; jlopezbustins@ub.edu (J.A.L.-B.); jmartinvide@ub.edu (J.M.-V.); joan.martinez.ar@gmail.com (J.M.-A.)
2 Regional Atmospheric Modelling (MAR) Group, Department of Physics, Regional Campus of International Excellence Campus Mare Nostrum (CEIR), University of Murcia, 30100 Murcia, Spain; amar.halifa@um.es
3 CRETUS, Non-Linear Physics Group, University of Santiago de Compostela, 15705 Santiago de Compostela, Spain; damian.insua@usc.es
4 Snow and Mountain Research Center of Andorra (CENMA-IEA), Av. Rocafort 21-23, AD600 Sant Julià de Lòria, Spain; ltrapero@iea.ad
5 Department of Geography, Autonomous University of Madrid, 28049 Madrid, Spain; roberto.serrano@uam.es
6 Department of Geography and Regional Planning, University of Zaragoza, 50009 Zaragoza, Spain; cuadrat@unizar.es
* Correspondence: mlemus@ub.edu

Citation: Lemus-Canovas, M.; Lopez-Bustins, J.A.; Martín-Vide, J.; Halifa-Marin, A.; Insua-Costa, D.; Martinez-Artigas, J.; Trapero, L.; Serrano-Notivoli, R.; Cuadrat, J.M. Characterisation of Extreme Precipitation Events in the Pyrenees: From the Local to the Synoptic Scale. *Atmosphere* **2021**, *12*, 665. https://doi.org/10.3390/atmos12060665

Academic Editor: Alexandre M. Ramos

Received: 26 April 2021
Accepted: 19 May 2021
Published: 22 May 2021

Abstract: Mountain systems within the Mediterranean region, e.g., the Pyrenees, are very sensitive to climate change. In the present study, we quantified the magnitude of extreme precipitation events and the number of days with torrential precipitation (daily precipitation $\geq$ 100 mm) in all the rain gauges available in the Pyrenees for the 1981–2015 period, analyzing the contribution of the synoptic scale in this type of event. The easternmost (under Mediterranean influence) and north-westernmost (under Atlantic influence) areas of the Pyrenees registered the highest number of torrential events. The heaviest events are expected in the eastern part, i.e., 400 mm day^{-1} for a return period of 200 years. Northerly advections over the Iberian Peninsula, which present a low zonal index, i.e., implying a stronger meridional component, give rise to torrential events over the western Pyrenees; and easterly advections favour extreme precipitation over the eastern Pyrenees. The air mass travels a long way, from the east coast of North America, bringing heavy rainfall to the western Pyrenees. In the case of the torrential events over the eastern Pyrenees, the trajectory of the air mass causing the events in these areas is very short and originates in the Mediterranean Basin. The North Atlantic Oscillation (NAO) index has no influence upon the occurrence of torrential events in the Pyrenees, but these events are closely related to certain Mediterranean teleconnections such as the Western Mediterranean Oscillation (WeMO).

Keywords: backward trajectory; extreme precipitation; Mediterranean region; Pyrenees; return period; teleconnection indices; weather type

1. Introduction

The climate of the Pyrenees, in southwestern Europe, is especially diverse, due to the orographic complexity of the sector. The Pyrenees are located in the geographical transition between the wet mild domain of the mid-latitudes and the arid area of the subtropical anticyclone belt. Both its marked topography and its location between two climatically differentiated basins, the Mediterranean and Atlantic basins, mean that this mountain area presents a highly variable climate. The precipitation variability in this area has been extensively studied [1–3] since it is clearly associated with different natural hazards in the

Pyrenees, such as avalanches [4–6], heavy snowfall [7–9], or flood events [10–12], among many others.

These natural hazards, particularly floods, can be triggered by torrential rainfall [13,14]. Insua-Costa et al. [14] were able to precisely characterise 1991 hazardous precipitation events into four main weather types and an extra one for low gradient pressure situations. This highlights the need to study atmospheric patterns involving this type of torrential event. However, most studies that characterize atmospheric patterns are based upon a "Circulation-to-Environment" approach; this means that the atmospheric circulation in a particular area is previously characterized and its implications for a given atmospheric/environmental variable at local scale are subsequently monitored [15,16]. Examples of this approach are widespread in the Pyrenees area. For example, Esteban et al. [17] modelled daily mean precipitation and temperature in Andorra for different circulation types, the latter obtained through principal component analysis (PCA) applied to an S-mode matrix [7] and subsequent clustering with k-means; similarly, Lemus-Canovas [18] employed statistical regression techniques to perform a synoptic classification focused on SW Europe aimed at mapping the daily mean precipitation of each weather type over the whole Pyrenees. Other examples of this type of approach can be found in different parts of the Iberian Peninsula [19–23], frequently using the objective Lamb approach [19,24]. However, another approach for characterising atmospheric patterns related to torrential events is known as "Environment-to-Circulation". It involves selecting days of interest (e.g., days with precipitation $\geq$100 mm) and creating a synoptic classification with these torrential days [14], or simply averaging the synoptic variable of interest on the days in which a given threshold is surpassed at the surface in order to finally perform a synoptic composite [25]. This type of approach has been applied to NE Iberia [26], Iberia [27], Southern Europe [14,28] and to other areas of the world, such as Japan [29] and Northern Chile [30], among others. In the abovementioned studies [14,26,27], the most commonly used approach to classify these extreme events is a PCA applied to a T-mode matrix. However, it has never been applied to the whole Pyrenees sector, a fact that constitutes a knowledge gap in relation to the synoptic characterization of torrential events in this region. Precisely, heavy precipitation is the product of two significant factors: a large amount of water vapour in the atmosphere and the upward flow of air, which generates the condensation of water vapour and subsequent precipitation. The Clausius–Clapeyron equation [31] provides a strong thermodynamic relationship between temperature and water vapour. Future climate projections indicate a greater increase in extreme precipitation than in the mean annual total precipitation [32].

In this sense, the main objective of this study involves describing in detail the spatial and temporal behavior of torrential rainfall in the Pyrenees, in order to subsequently synoptically characterize such events and to establish the origin of the air masses driving such episodes. The specific objectives are: (i) to compute the annual maximum daily precipitation values from different return periods, and to quantify the number of days with torrential precipitation (daily precipitation $\geq$ 100 mm) and establish its temporality; (ii) to characterize the large-scale atmospheric patterns causing such torrential events ($\geq$100 mm); and (iii) to employ a backward trajectory analysis in order to determine the main trajectories of the air masses giving rise to the occurrence of torrential events.

2. Data and Methods

2.1. Data

Daily precipitation was extracted from the database of the CLIMPY Project (Characterisation of evolution of climate and provision of information for adaptation in the Pyrenees), a transboundary project intended to establish a detailed analysis of recent trends in temperature, precipitation, and snow cover in the Pyrenees [33]. Only the weather stations containing at least 90% of the data in the 1981–2015 period (158 in total) were considered when counting the torrential events (Figure 1). For the computation of return periods, we only used observatories providing a complete record in their data series. All series were

subjected to a previous quality control process described in Serrano-Notivoli et al. [34]. The spatial and altitudinal distribution of weather stations is generally homogeneous, except for the central Pyrenees, for which no historical records meet the criterion for data availability.

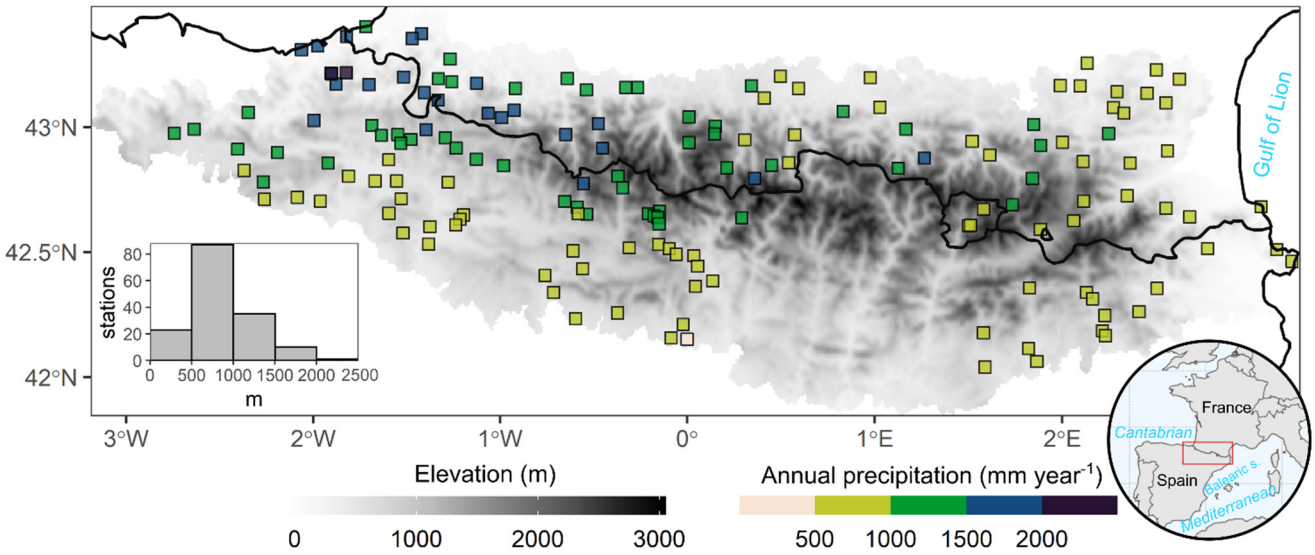

Figure 1. Pyrenees location (**bottom right**), elevation (**greyscale legend**) and spatial distribution of the rain gauges in the Pyrenees area and annual amounts of precipitation (**coloured squares**). At bottom left, a histogram shows the frequency of rain gauges per range of elevation. The black line shows the national boundaries.

We used mean sea level pressure (mslp), temperature at 850 hPa (t850) and geopotential height at 500 hPa (z500) to compute the synoptic classification. These gridded variables were supplied by the ERA-5 reanalysis [35] by means of daily mean values, encompassing the area 30° N–60° N and 20° W–20° E at a horizontal resolution of 0.25° for the 1981–2015 period. Finally, backward trajectories were computed by means of the Hysplit model [36], fed by the NCEP/NCAR reanalysis database [37] at a horizontal spatial resolution of 2.5°.

Additionally, we analysed the Western Mediterranean Oscillation (WeMO) [38], the Mediterranean Oscillation (MO) [39], the Upper-Level Mediterranean Oscillation (ULMO) [40] and the North Atlantic Oscillation (NAO) [41]. They are all at daily resolution and for the 1981–2015 period. The MO, NAO and WeMO indices were provided by the Climatic Research Unit (https://crudata.uea.ac.uk/cru/data/pci.htm, accessed on 16 May 2021), whilst the ULMO was furnished by the authors.

2.2. Analysis of Extreme Events and Definition of Torrential Events

To estimate the return level of precipitation given a specific return period (RP), we employed the generalized extreme value (GEV) distribution for extreme events. The cumulative distribution function of the GEV results from combining the Frechet, Gumbel and Weibull families of distributions in one single distribution function:

$$F(x) = \exp\left\{-\left[1+\xi\left(\frac{x-\mu}{\sigma}\right)\right]^{-1/\xi}\right\} \quad (1)$$

where three parameters (ξ, μ and σ) represent the shape, location and scale of the distribution function, respectively. The σ and $1 + \xi(x - \mu)/\sigma$ must be greater than zero. The specification of ξ will determine the behavior of the tail of the distribution so that, depending on the value of this parameter, any of the following distributions might be obtained:

- $\xi > 0$ giving the heavy-tailed (Frechet) case;
- $\xi = 0$ giving the light-tailed (Gumbel) case. For this case:

$$F(x) = \exp\left\{-\exp\left[-\left(\frac{x-\mu}{\sigma}\right)\right]\right\} \quad (2)$$

- $\xi < 0$ giving the bounded-tailed (Weibull) case.

The GEV family of distributions enables the annual daily maximum precipitation to be modelled with the use of the block maxima approach. This procedure consists of grouping the data into blocks of equal size—one for each year—and then fitting the GEV distribution to the set of maxima corresponding to each of the blocks.

Apart from the modeling of extremes by means of GEV analysis, torrential events were defined as days when daily accumulated precipitation ≥100 mm. A precipitation equal to or greater than 100 mm day^{-1} was the threshold used to identify heavy rainfall events in Catalonia (NE Iberia) [26,42,43], associated with an increase in soil erosion processes [44]. In addition, the precipitation threshold equal or greater than 100 mm day^{-1} could be considered equivalent to the 95th percentile or above across all precipitation series of the study area (Figure S1 of the Supplementary Material).

2.3. Synoptic Classification Approach and Circulation Composites

We applied a PCA to a T-mode (temporal) matrix of mslp, t850 and z500, where the variables (columns) were the 220 days displaying torrential precipitation and the cases (rows) were the grid points of ERA-5. Once the PCA was applied to the standardized data matrix, new variables were obtained, the principal components (PCs), which are linear combinations of the original variables. Subsequently, the PCs explaining most of the variance of the original data needed to be retained by conducting a Scree Test [45]. Once the PCs were retained, the components were rotated with a Varimax rotation in order to readjust the orthogonal combination of each PC to obtain a greater variance, which was explained by those PCs of lesser rank [46]. From the rotated PCs, we obtained the loading, i.e., the correlation matrix, which indicates the degree of correlation of each day with respect to each PC. In this sense, the assignment of each day to each of the PCs is based on the value of maximum positive correlation and minimum negative correlation. For example, day 1 is assigned to the highest absolute correlation, but subsequently retains the correlation symbol. For this reason, PC1 may be split into two groups, one for the days with the highest positive maximum correlation, and one for the days presenting the lowest negative correlation. This means that, if we retain 5 PCs, up to 10 weather types can be obtained. We used the R package synoptReg [15] to develop the synoptic classification.

To complement the explanation of the synoptic mechanisms that lead to such torrential events, we computed the vertically integrated water vapor transport (IVT) between the 1000 and 300 hPa levels, following the methodology proposed by Lavers et al. [47]:

$$IVT = \sqrt{\left(\frac{1}{g}\int_{1000hPa}^{300hPa} q{\cdot}u{\cdot}dp\right)^2 + \left(\frac{1}{g}\int_{1000hPa}^{300hPa} q{\cdot}v{\cdot}dp\right)^2} \quad (3)$$

where q is the specific humidity (kg kg^{-1}); u and v are the layer-averaged zonal and meridional winds (m s^{-1}), respectively; g is the acceleration due to gravity (m s^{-2}); and p is the pressure difference between two adjacent pressure levels (Pa).

Furthermore, the meridional and zonal components of the wind at 300 hPa were used to identify the positions of the polar jet during these torrential events.

2.4. Hysplit Model

The Hybrid Single Particle Lagrangian Integrated Trajectory (HYSPLIT) model enables trajectories of simple air particles to be computed, and their transport, dispersion, and deposition [36] to be simulated. It is one of the most widely used models in the atmospheric sciences to determine the origin of air masses and to define the source–receptor relationship [48,49]. The use of gridded climate data permits the HYSPLIT model to define the trajectory air parcel arriving at a specific location at a specific time on a specific date.

We used the NOAA Hysplit model to determine the backward trajectories of episodes equal to or greater than 100 mm at Darnius (easternmost Pyrenees) and Artikutza (westernmost Pyrenees); both of these locations possess the highest number of records above this threshold and in opposite geographical locations within the study area.

Meteorological data were obtained from the NCEP/NCAR Reanalysis database [37] with 2.5° resolution. The set-up of the model was based on mean sea level pressure, 850 hPa, and 500 hPa. With these settings, we obtained the back trajectories for 96 h, departing at 00, 06, 12 and 18 h for each of the torrential days during the 1981–2015 period.

3. Results and Discussion

3.1. Maximum Daily Precipitation for Different Return Periods

The GEV analysis provided the return levels for six RPs: 5, 10, 20, 50, 100 and 200 years (Figure 2). For a 5-year RP, maximum daily precipitation was generally estimated to be below 100 mm, except in the extreme east, where values of 150 mm day^{-1} were reached. The eastern Pyrenees is one of the areas receiving the most torrential episodes on the Iberian Peninsula [14,43]. For a 10-year RP, 100 mm day^{-1} was generally reached throughout the region, with over 150 mm per day in the northeastern Pyrenees. The same spatial pattern was repeated for a 20-year RP, with the northeastern region exceeding 200 mm day^{-1}. Interestingly, values of 150 mm day^{-1} were recorded in different observatories in the northwest of the study area. For the most extreme RPs (RP 100 and RP 200), 300 mm day^{-1} was easily exceeded on the eastern slope of the Pyrenees. Even in the extreme northeast, over 400 mm day^{-1} was recorded for a RP of 200 years. In the rest of the study area, several observatories in the west and south stand out, providing 200–300 mm day^{-1} for a 200-year RP. Intense NW wind circulation over the Iberian Peninsula can lead to heavy rainfall in non-typical Mediterranean climates such as that of the Western Pyrenees [39]. The areas presenting the lowest extremes were the central part of the northern slopes of the Pyrenees, where different observatories did not reach 150 mm day^{-1} for the highest RP (200 years).

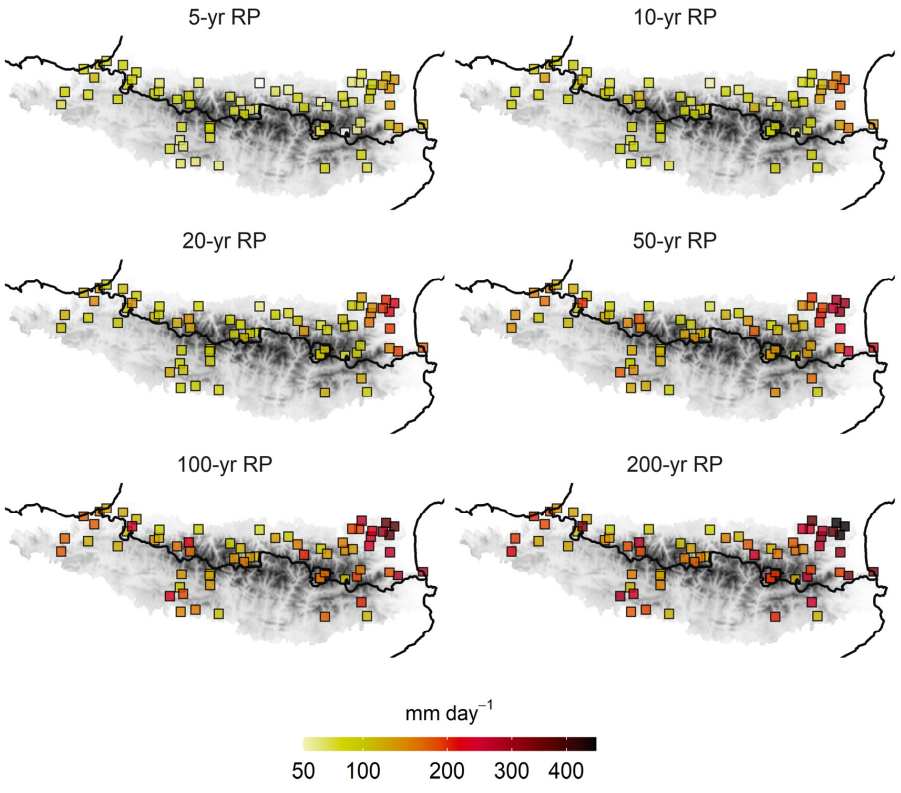

Figure 2. Return levels of maximum daily precipitation per year for 6 different return periods (RPs): 5, 10, 20, 50, 100 and 200 years. Only the stations with the complete series were used.

3.2. Characterisation of Torrential Events: Spatial Distribution and Seasonality

The frequency of torrential events exhibits certain well-defined spatial patterns. Figure 3a clearly shows the dependence on distance to the sea of the days with amounts equal to or greater than 100 mm in the eastern part of the study area [50]. Moreover, in the extreme west, the maximum was located slightly southward of the axis of the mountain range (Artikutza), whereas in the extreme east the torrential episodes spread over a wider strip, both north and south of the axis of the mountain range, with a maximum in Darnius (Figure 3a). The latter phenomenon might be caused by the N–S direction of the coast, which is at a right angle to the mountain range's W–E axis [51]. The remaining rain gauges depend, to a certain degree, upon altitude. The observatories situated at higher elevations also present a higher number of torrential days as a result of convective precipitation in summer.

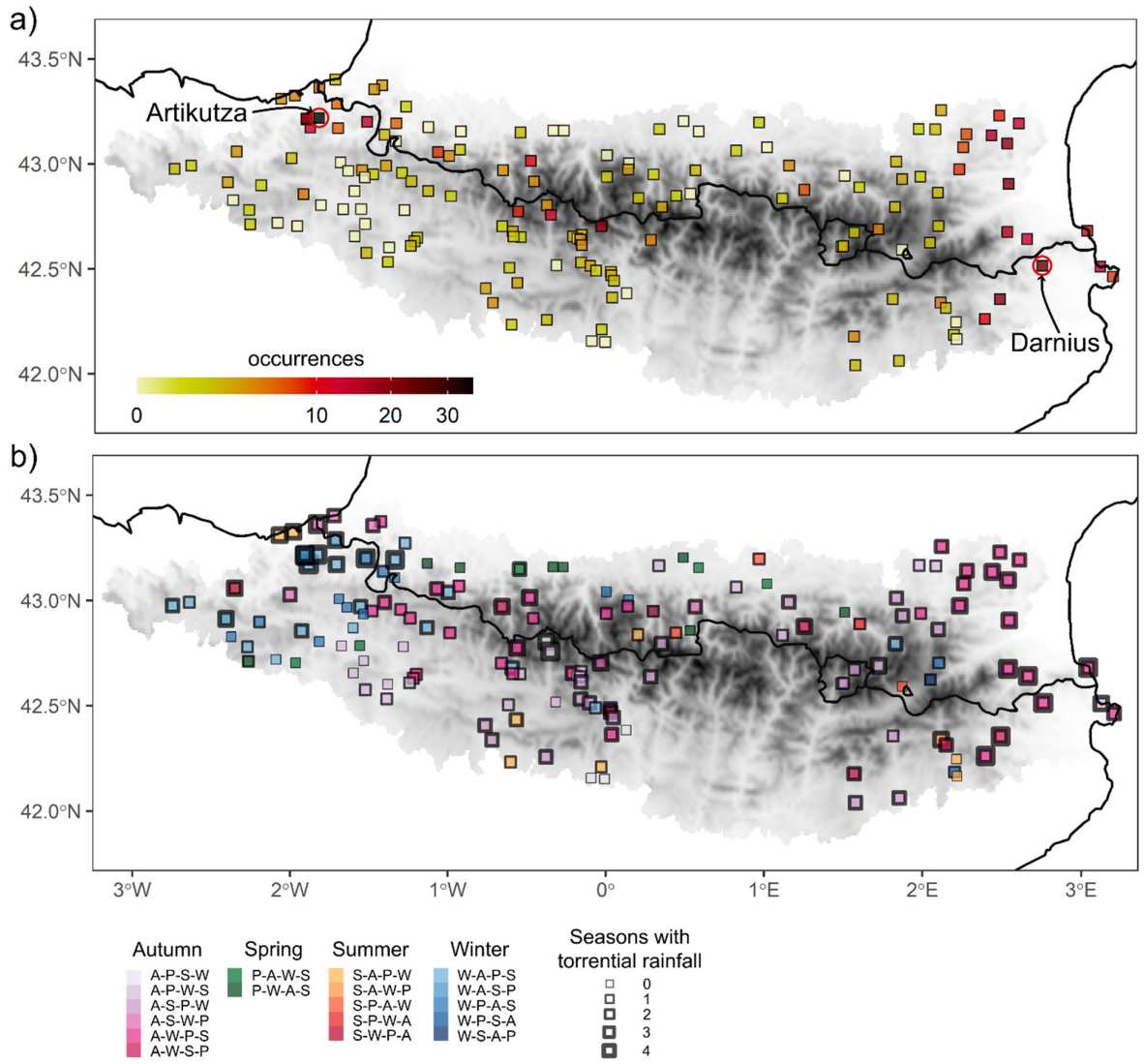

Figure 3. (**a**) Number of days with torrential rainfall for the 1981–2015 period. Location of Artikutza and Darnius rain gauges, which present the greatest number of torrential events (they are, therefore, used to calculate the backward trajectories with the Hysplit model in Section 3.4). (**b**) Seasonal torrential regimes in the Pyrenees: A (autumn), P (spring), S (summer), and W (winter). The border thickness of the box indicates the number of seasons with torrential rainfall, and the boxes with the thickest line, therefore, correspond to weather stations that recorded at least one event in winter as well as in spring, summer and autumn.

Figure 3b shows a great variety of days with seasonally distributed torrential precipitation in the Pyrenees, a fact that reinforces the pluviometric complexity of the study area. In addition, episodes are observed to be prevalent in winter in the westernmost extreme, when NW advections are frequent [18], and in autumn in the extreme east, when easterly flows are more intense [50]. On the Mediterranean coast, all seasons are perceived to present at least one episode of torrential rain. Moreover, the colour purple symbolises the season of the year with the most torrential events, autumn, followed by winter in most of rain gauges located in the area closest to the coastline. At the opposite end (west) of the study area, a large number of observatories indicate that the torrential event occurs mainly in winter, with a transition to the autumn months towards the centre and south of the study area. Spring and summer, however, have a lesser impact, only affecting the northernmost central part of the region and presenting no torrential episodes. Furthermore, the springtime precipitation regime has become less predominant over the Iberian Peninsula during the last few decades (1976–2005) due to an increase in autumn rainfall, with respect to the 1946–1975 period [52].

3.3. Large-Scale Attribution of Torrential Events

Based on the methodology described in Section 2.3, we obtained nine weather types (WT), since five PCs were retained, accounting for 80 % of the variance of the original data (Figure S2 of the Supplementary Material). Figure 4 presents the spatial representation of the mslp, t850 and z500 of the WTs. All of the synoptic patterns presented resulted in days with 100 mm or greater in a rain gauge. The high number of synoptic patterns (nine) is due to the geographical and pluviometric diversity of the study area, already seen in the previous maps (Figures 2 and 3), and the synoptic variety, which for this kind of event is already known in areas of the northeast of the Iberian Peninsula [26].

The most frequent synoptic pattern in the occurrence of torrential events is WT1, which is associated with 19.1% of the cases, and with an unequivocal seasonality in the cold half of the year (Figure S3 of the Supplementary Material). This WT is characterized by a low-pressure system near the surface in the Balearic Sea, which drives moist maritime winds to the easternmost area of the Pyrenees (Figure 5). In addition, this evident surface low is also accompanied by a low at 500 hPa and a below-average temperature at 850 hPa over the Iberian Peninsula. This WT1 is very well characterized by the negative phase of the WeMO (Figure 6) due to the combination of low surface pressure on the south of the Iberian Peninsula with high pressure in northern Italy in this type of situation [26]. Moreover, the MO presents clearly negative values when such a situation occurs. Figure 5 shows that for WT1 there is evidence of moisture advection in the extreme east of the Pyrenees, which increases the potential of these torrential events [53], whilst a meridional position of the jet stream with a north direction can be observed. Precisely, this WT1 is at its most effective in the eastern Pyrenees (Figure 7b), as well as in other areas of the western façade of the Iberian Peninsula [54], causing a large number of torrential events (Figure 7a). Due to its winter seasonality and negative temperature anomalies, the WT1 causes a significant fraction of these episodes to occur as snowfall [55]. WT2 (Figure 4) is characterized by a trough located at the northwest of the Iberian Peninsula and an increase in pressure towards eastern Europe, a situation which is very well characterized by both the WeMO and MO. The location of the low favours warm and moist air advection from the Mediterranean over the study area, with an increase in IVT intensity (Figure 5), giving rise to prefrontal precipitation [53]. This pattern can appear throughout the year, but its maximum frequency is in mid-autumn (Figure S3). Torrential rainfall during this synoptic situation is concentrated on the southern slope, as shown in Figure 7, as a result of this important moisture that was advected from subtropical origin. In fact, Insua-Costa et al. [56] recently showed that moisture advected via an atmospheric river from the tropical and subtropical Atlantic played a major role in a well-known case of this type, the November 1982 flood event. In addition, this type of episode has aroused interest in studying the physical mechanisms of high precipitation events related to this

synoptic pattern in the eastern Pyrenees [10,11]. WT3 and WT4 exhibit similar surface characteristics, although the former occurs in late summer and during autumn, and the latter mainly during the winter months (Figure S3). In both cases, north-northwesterly winds over the Pyrenees are involved. However, in WT4 the main action centres driving the northerly advection are more clearly defined: the Azores anticyclone in the west of the Iberian Peninsula and a depression in Italy, favouring positive values of the WeMO index (Figure 6). This indicates a stronger advection in WT4 than in WT3. The aforementioned phenomenon can also be observed depending on the intensity and direction of the IVT (Figure 5) and with a wind trajectory at 300 hPa (Figure S4), which is perpendicular to the Pyrenees, mainly in WT4. This brings abundant precipitation to most of the northern façade of the region (see Figure 7). Precisely, WT3 displays low pressure gradient over the Pyrenees, a common occurrence in summertime in this area when convective activity in the whole area is dominant [17]. Because of that, torrential situations under this weather type might not be persistent but rather stormy, a situation also defined in Pineda et al. [57].

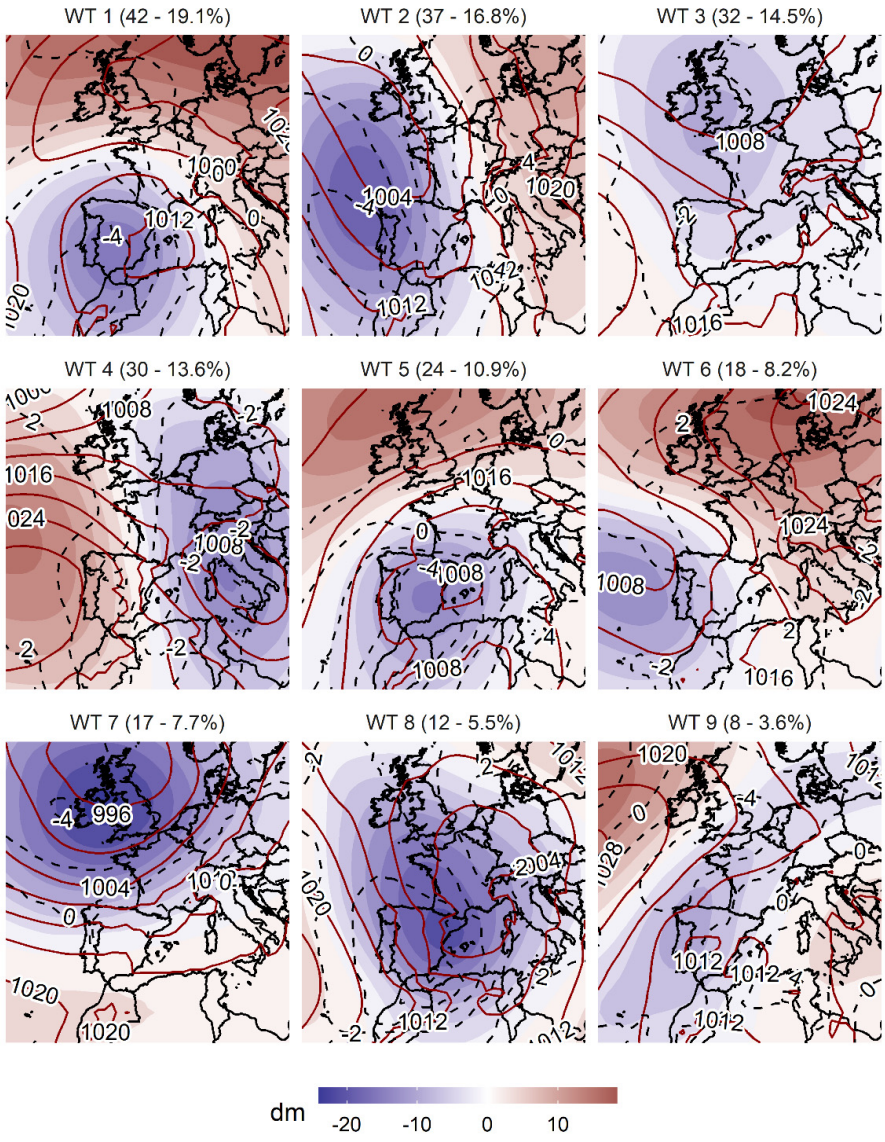

Figure 4. Mean sea level pressure (dark red contours, hPa), 500 hPa geopotential height anomalies (shaded colours, dam) and 850 hPa temperature anomalies (dashed contours) of the nine most frequent weather types associated with torrential precipitation in the western Mediterranean region. Above each map, the number of days assigned to each synoptic pattern and their percentages with respect to the total are shown in parentheses.

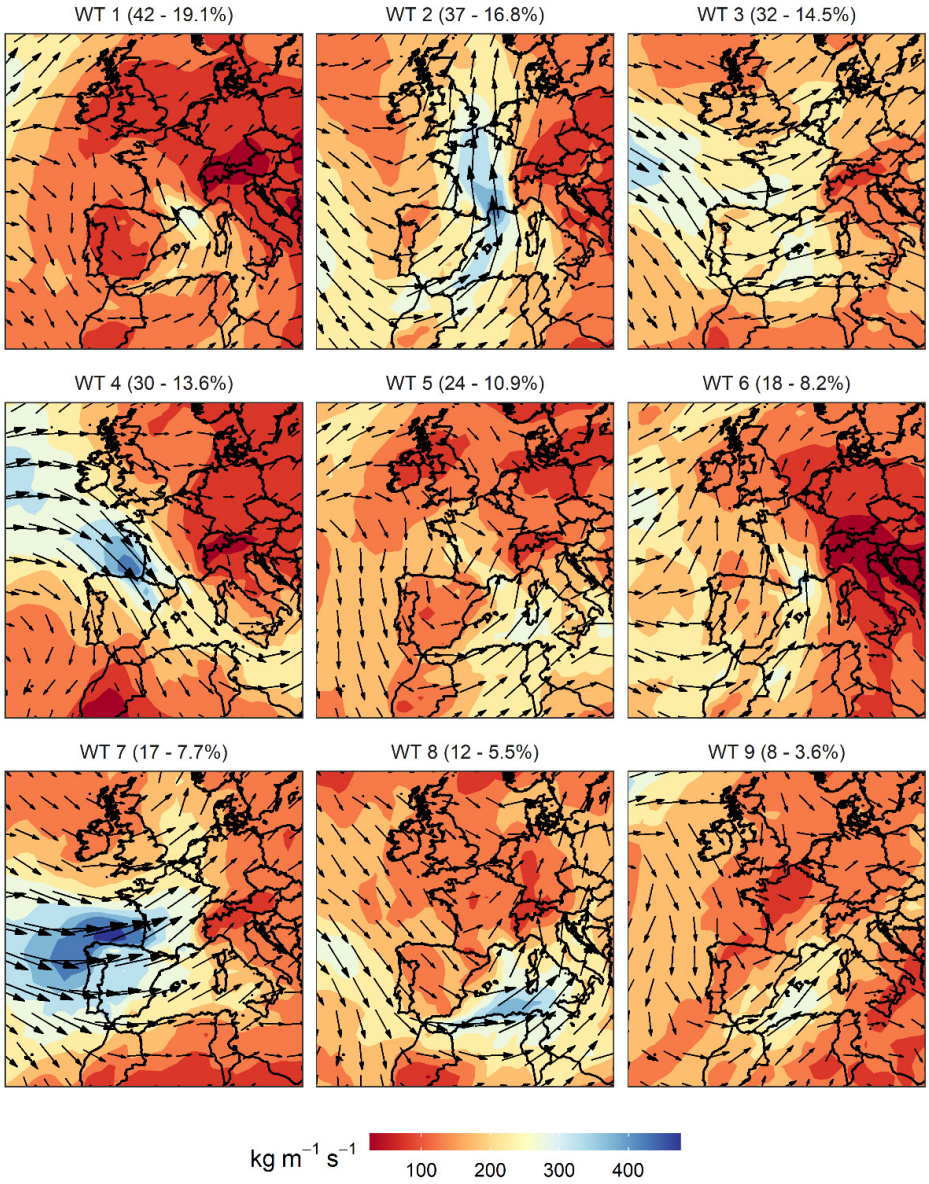

Figure 5. Vertically integrated water vapor transport (IVT) intensity (shaded colours, kg m^{-1} s^{-1}) and direction (vectors) of the 9 most frequent atmospheric patterns associated with torrential precipitation in the western Mediterranean region. Above each map, the number of days assigned to each synoptic pattern and their percentages with respect to the total are shown in parentheses.

As opposed to WT1, WT5 occurs more frequently in late spring and early autumn (Figure S3). This pattern reveals a surface depression over the Balearic Sea driving an east-northeasterly advection in the eastern area of the Pyrenees and a north-northeasterly advection in the westernmost area, favoring two poles of precipitation maxima in both areas (map 5, Figure 7b). Such a situation is captured very well by the ULMO teleconnection pattern, which represents the MO dipole, but at 500 hPa (Figure 5). WT6, with a depression to the northwest of the peninsula and an anticyclone in central Europe, favours a warm air advection from the south-southeast with a significant moisture content (Figure 5) that favors abundant precipitation in the eastern coastal area (Figure 7b), and also in the southernmost mountainous sector of the study area. This is one of the situations that is captured well by the negative phase of the WeMO (Figure 6), and it concisely explains the occurrence of torrential-type events in the extreme northeast of the Iberian Peninsula [49], and their pluviometric variability in general [51,58]. WT7 presents a high zonal gradi-

ent that favours westerly flows over the Iberian Peninsula with a long-lasting advection over the ocean, which causes significant moist advection over the Atlantic façade; this exhibits a temporal frequency centred in the months of October, November and December (Figure S3). This situation promotes notable precipitation in the western half of the Pyrenees, whereas, in the eastern half, this contribution is truncated because the advection loses all its moisture due to an adiabatic process of leeward compression. For this situation, no teleconnection pattern clearly defines the aforementioned atmospheric pattern, a fact also reported in Merino et al. [53]. WT8 exemplifies a widespread depressional situation centred over France, both on the surface and at 500 hPa, driving a northerly advection over the whole Pyrenees range; this advection is reinforced by a southward shift of the jet stream (Figure S4), and, by default, a displacement of the polar vortex from the Arctic region. The MO and ULMO provide the best definition of such a situation: a large depression over the western Mediterranean and an anticyclonic centre over the eastern Mediterranean. This kind of configuration causes widespread precipitation along the northern slope of the Pyrenees (Figure 7b), and, in some rain gauges in this northernmost part of the Pyrenees, this is the WT that causes the most torrential episodes (Figure 7a). Finally, WT9 presents a more residual frequency, and is characterised by a weak depression in the southeast of the peninsula that drives southeasterly surface winds transporting significant moisture and distributes the highest amount of precipitation over the southeastern extreme of the Pyrenees (Figure 7b).

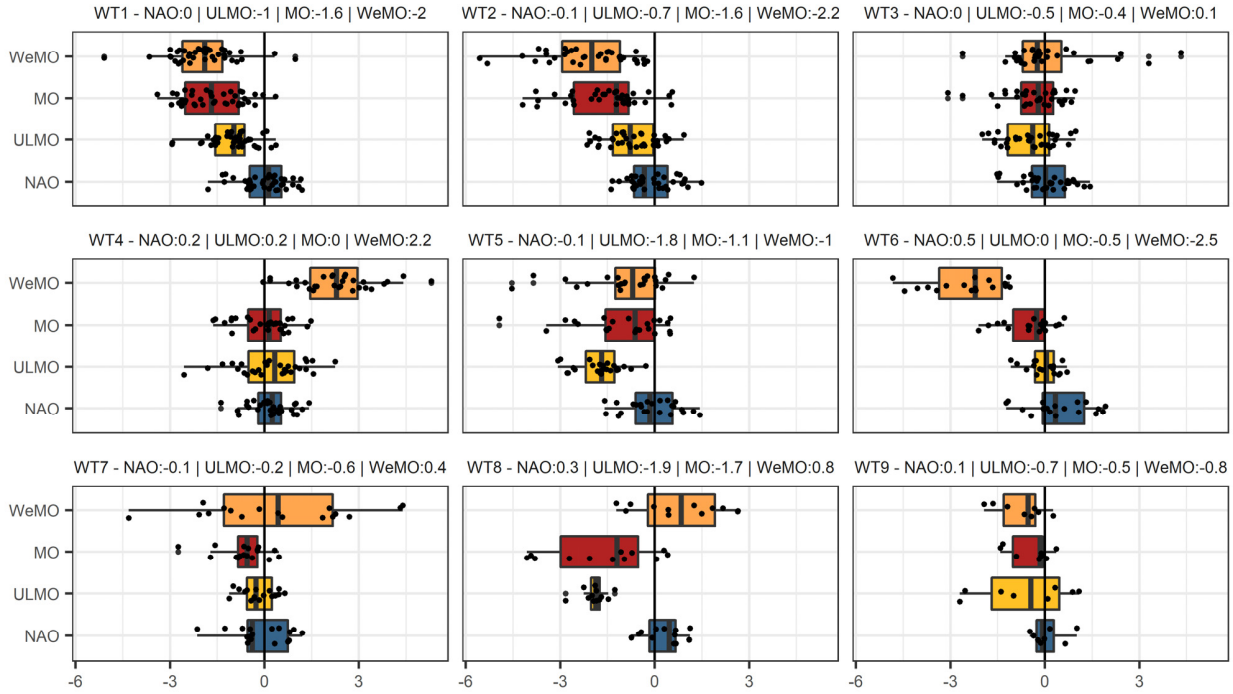

Figure 6. Distribution of daily values of the teleconnection indices for each weather type (WT). The mean value of each teleconnection index for each WT is shown in the header of each plot.

These results hardly reveal any influence of the NAO in any of the situations causing torrential precipitation events in the Pyrenees. Extreme precipitation events in northeastern Spain are not associated with the NAO index values [50]. The main influence of the NAO on rainfall over the Iberian Peninsula is observed in the central and southwestern parts [27,59]. Esteban et al. [60] found that winter rainfall over the southern central Pyrenees comes under the influence of the negative phase of the NAO, which is associated with southerly and southwesterly synoptic circulation (WT2 in Figure 7a). This can also be seen in the highest values of mean daily precipitation (25–50 mm) in WT2 (Figure 7b), which are mostly concentrated over the central area of the southern slope of the Pyrenees. The

amount reached for a 200-yr RP over the central-south slope of the Pyrenees is rather low (about 200 mm) in comparison with that amount over the extreme east (about 400 mm). This fact denotes a climate typically under Atlantic influence (NAO) in the central-south Pyrenees and a highly variable climate under Mediterranean influence (WeMO) in the easternmost Pyrenees. Esteban et al. [60] found no statistically significant correlation between precipitation over the north slope of the Pyrenees and the NAO index, a fact that is likely a result of the orography barrier.

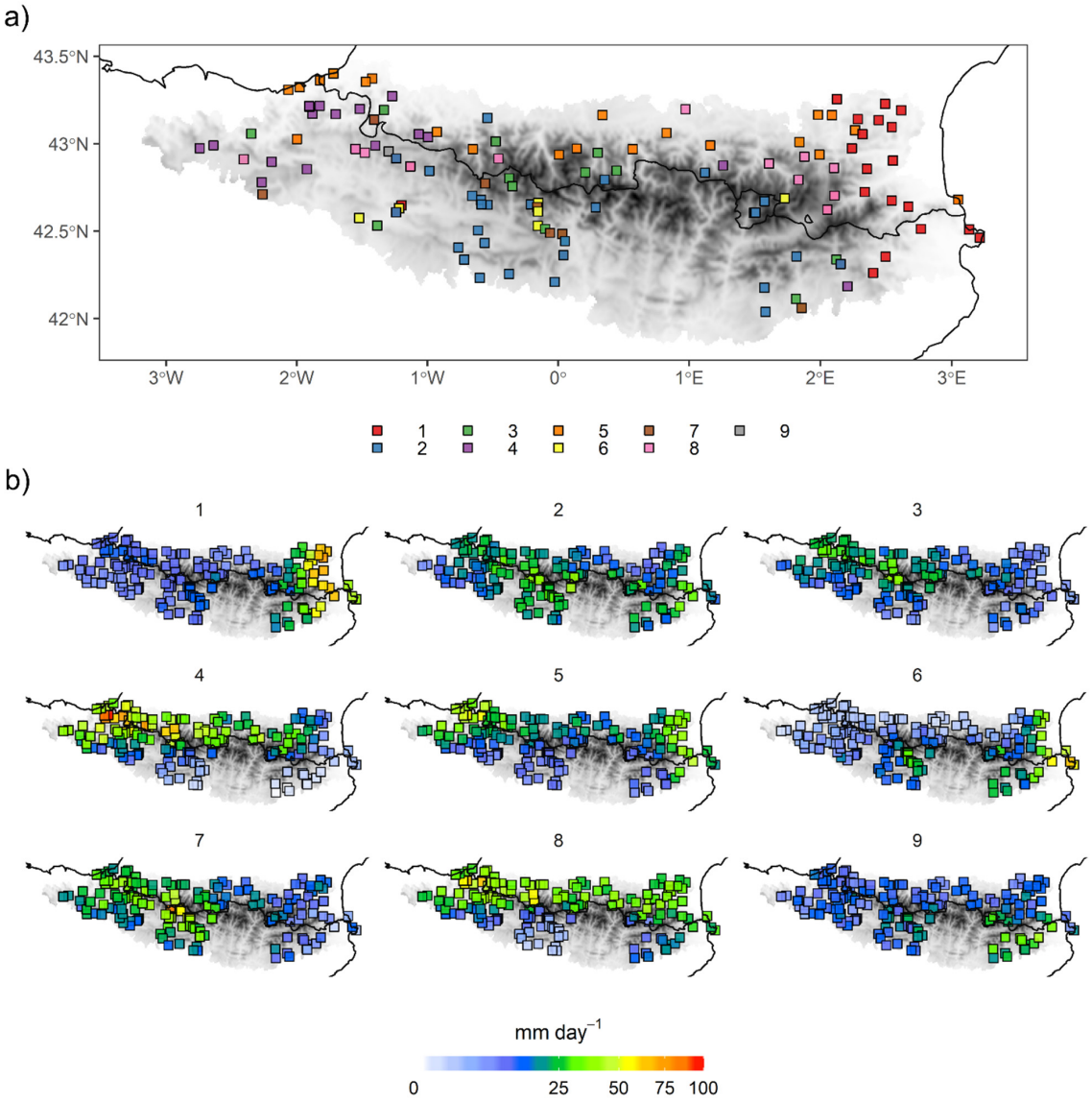

Figure 7. (**a**) Weather type (WT) with the maximum frequency in each rain gauge (each colour represents one of the nine WTs); (**b**) mean daily precipitation for each of the WTs.

3.4. Backward Trajectory Analysis

There is an unequivocal contrast between the backward trajectories of Artikutza and Darnius for the three altitudinal layers: 500 hPa (Figure 8a), 850 hPa (Figure 8b), and surface (Figure 8c). The first rain gauge is located at the northwestern end of the Pyrenees (Figure 3a), very close to the Atlantic coast, which implies a clear influence of the westerlies and the rapid westerly circulation. The second rain gauge is at the opposite (eastern) end of the Pyrenees, very close to the mediterranean coast (Figure 3a); it is in the lee side of the westerly flows and is clearly characterized by the Mediterranean climate. Most of

the trajectories at 500 hPa (Figure 8a) for Artikutza originate in the North Atlantic Ocean, implying a long maritime trajectory of the air particles, which come to favour synoptic patterns related to intense rainfall. Darnius is clearly different from the Artikutza, because at a height of 500 hPa a long trajectory is to be expected, but results reveal that most of the trajectories at that height are short, mainly of Mediterranean and subtropical Atlantic origins. In general, for the case of Darnius, the trajectory is short, but quite variable with regard to its origin, as noted in Pastor et al. [61], but for the Valencia region (Spain). The trajectories at 850 hPa (Figure 8b) do not reveal significant differences with respect to those at 500 hPa. They are shorter than those at 500 hPa as a result of atmospheric dynamics and surface friction. In the case of Darnius, it is worth noting that almost all the trajectories at 850 hPa are of Mediterranean origin (see WT1, WT5, and WT9 in Figure 4) or come from North Africa (see WT2 and WT6 in Figure 4). Finally, at the surface level (Figure 8c), the shortest trajectories are detected; these are clearly of North Atlantic origin in the case of Artikutza, which are clearly related to WT4 and WT7, although different situations exist which are characterized by trajectories of northern and even northeastern origin travelling over the Cantabrian Sea. In the case of Darnius, practically all the trajectories originate between the Balearic Sea, the Gulf of Lion and the Italian Peninsula; very occasionally, some trajectories originate in the North Atlantic. The surface trajectories for Darnius reveal a strong dependence on the local and mesoscale environments in the Mediterranean basin, as opposed to the rapid surface air circulation over Artikutza coming from a distant location, such as western Canada. Another remarkable fact involves the greater homogeneity in Artikutza than in Darnius at all levels with regard to the direction of the backward trajectories; these are mostly zonal and present very diverse origins.

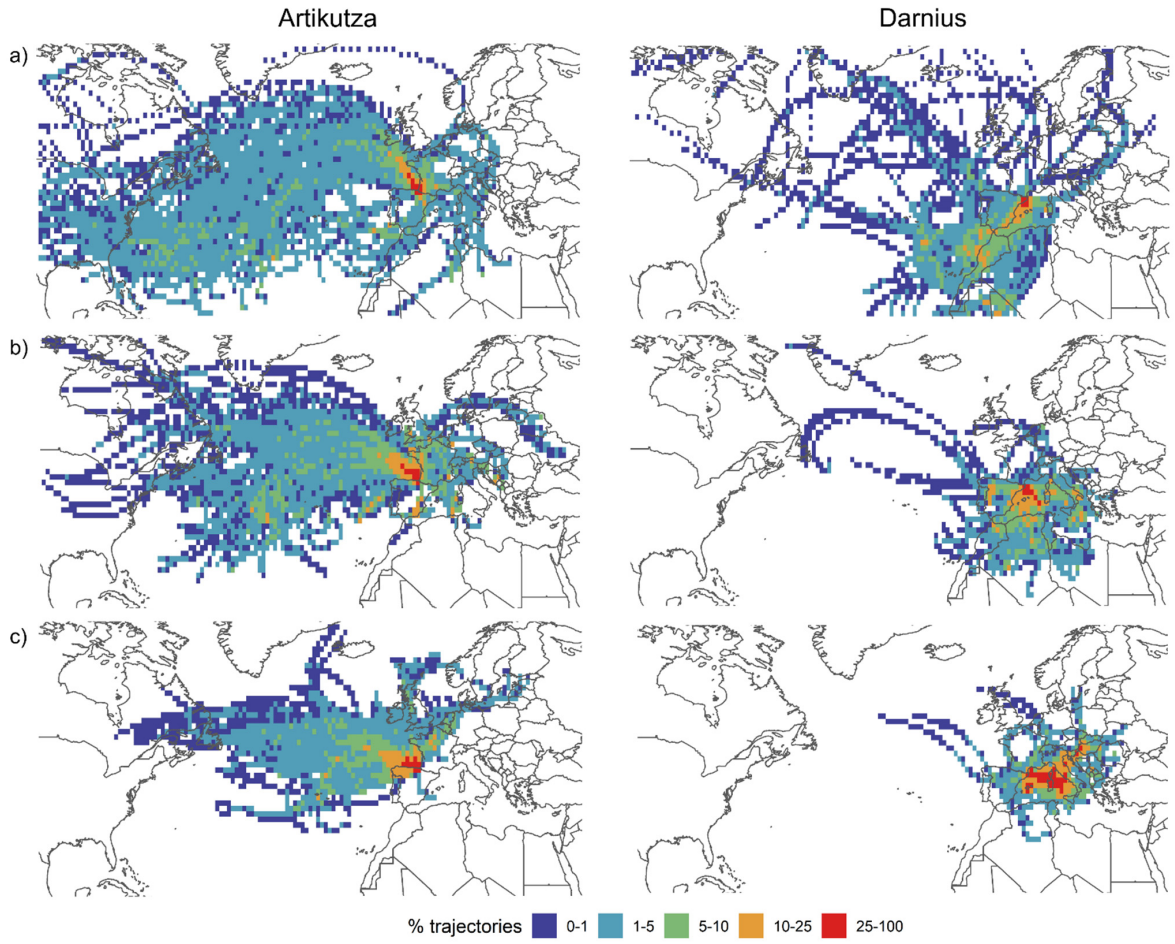

Figure 8. Backward trajectories for Artikutza (NW of the study area) and Darnius (E of the study area) for their respective days with torrential rainfall. The trajectories were computed for three different altitudinal layers: (**a**) 500 hPa, (**b**) 850 hPa and (**c**) surface.

4. Conclusions

Estimation of return periods revealed that, in the easternmost area of the Pyrenees, there is a high risk of events greater than 150 mm day^{-1} for return periods of only 5 years. For extreme return periods (200 years), the amounts are extremely high in this eastern area, reaching 400 mm day^{-1}. It is specifically this eastern area and the extreme northwest area that provide the most records equal to or greater than 100 mm, i.e., torrential rainfall.

Together with the climatic and geographic complexity of this region, a wide range of synoptic patterns accounts for these torrential events. Thus, in the northern and western areas of the Pyrenees, the main situations causing torrential events are characterized by advection from the north and northeast at surface level and a meridional circulation of the jet stream over the study area, usually accompanied by significant moisture content. The westerlies can also cause torrential events when a deep depression is located over the north of the Iberian Peninsula. This WT has a large air circulation over the North Atlantic, as shown by the analysis of the backward trajectories. In the central-southern sector of the study area, torrential rainfall is dominated by the second most recurrent WT, which is characterised by a low-pressure system in the northwest of the Iberian Peninsula, and which drives very moist southerly winds. On the other hand, the Mediterranean is subjected to the highest number of torrential events with low pressures over the western Mediterranean, which drive easterly and southeasterly winds over the Iberian Peninsula. Only one situation presented a significant number of torrential events; this was weakly defined at surface level due to cold air at high altitude during the summer season. In the easternmost area of the Pyrenees, the air masses that generate torrential rainfall present a short trajectory, coming from subtropical latitudes, in contrast with what happens in the westernmost area, where the path of the air masses is much longer and usually originates on the east coasts of North America and Canada. The heaviest precipitation in the Pyrenees is mainly monitored by the WeMO index: the eastern and northwestern areas come under the influence of the negative and positive phases of the WeMO, respectively (WT1 and WT4 in Figures 4 and 6). The NAO index has no effect upon the occurrence of torrential events in the Pyrenees, except for isolated areas on the southern façade of this mountain range.

Further research is required on these extreme precipitation events in Mediterranean mountain ranges such as the Pyrenees. This sector could be directly affected by climate change, with the risk of several associated natural hazards becoming more frequent.

Supplementary Materials: The following are available online at https://www.mdpi.com/article/10.3390/atmos12060665/s1, Figure S1: Scree test for the first 30 principal components (PCs). The red dots show the explained variance (%) for each principal component, while the black bars show the cumulative explained variance. Figure S2: Relative monthly frequencies in percentages of each weather type (WT) for the 1981–2015 period. Figure S3: Daily mean 300 hPa wind direction and speed (m s^{-1}) of the 9 most frequent weather types associated with torrential precipitation in the western Mediterranean region. Above each map, the number of days assigned to each synoptic pattern and their percentages with respect to the total are shown in parentheses.

Author Contributions: Conceptualization, M.L.-C., J.A.L.-B. and J.M.-V.; methodology, M.L.-C., J.A.L.-B. and J.M.-V.; validation, A.H.-M., D.I.-C., J.M.-A., L.T., R.S.-N. and J.M.C.; formal analysis, M.L.-C. and J.A.L.-B.; investigation, M.L.-C., J.A.L.-B. and J.M.-V.; data curation, M.L.-C. and R.S.-N.; writing—original draft preparation, M.L.-C., J.A.L.-B. and J.M.-V.; writing—review and editing, M.L.-C., J.A.L.-B., J.M.-V., D.I.-C., A.H.-M., J.M.-A., L.T., R.S.-N. and J.M.C.; supervision, L.T., D.I.-C., A.H.-M., J.M.-A. and J.M.C. All authors have read the manuscript and agreed to the published version of the manuscript.

Funding: The present study was conducted within the framework of the Climatology Group of the University of Barcelona (2017 SGR 1362, Catalan Government) and the Spanish CLICES project (CGL2017-83866-C3-2-R, AEI/FEDER, UE). M.L.-C. was awarded a pre-doctoral FPU Grant (FPU2017/02166) from the Spanish Ministry of Science, Innovation and Universities. R.S.-N. and J.M.C. are partially supported by the Government of Aragón through the "Program of research groups" (group H38, "Clima, Agua, Cambio Global, y Sistemas Naturales").

Institutional Review Board Statement: Not applicable.

Informed Consent Statement: Not applicable.

Data Availability Statement: Not applicable.

Acknowledgments: The daily precipitation data were provided by the CLIMPY Project (Characterisation of evolution of climate and provision of information for adaptation in Pyrenees) (2014–2020 INTERREG V-A Spain–France–Andorra, POCTEFA).

Conflicts of Interest: The authors declare that no conflict of interest exists.

References

1. Beguería, S.; Vicente-Serrano, S.M.; López-Moreno, J.I.; García-Ruiz, J.M. Annual and seasonal mapping of peak intensity, magnitude and duration of extreme precipitation events across a climatic gradient, northeast Spain. *Int. J. Clim.* **2009**, *29*, 1759–1779. [CrossRef]
2. Vicente-Serrano, S.M.; Beguería, S.; López-Moreno, J.I.; El Kenawy, A.M.; Angulo-Martínez, M. Daily atmospheric circulation events and extreme precipitation risk in northeast Spain: Role of the North Atlantic Oscillation, the Western Mediterranean Oscillation, and the Mediterranean Oscillation. *J. Geophys. Res.* **2009**, *114*, D08106. [CrossRef]
3. Buisan, S.T.; Saz, M.A.; López-Moreno, J.I. Spatial and temporal variability of winter snow and precipitation days in the western and central Spanish Pyrenees. *Int. J. Clim.* **2015**, *35*, 259–274. [CrossRef]
4. García-Sellés, C.; Peña, J.C.; Martí, G.; Oller, P.; Martínez, P. WeMOI and NAOi influence on major avalanche activity in the Eastern Pyrenees. *Cold Reg. Sci. Technol.* **2010**, *64*, 137–145. [CrossRef]
5. Oller, P.; Muntán, E.; García-Sellés, C.; Furdada, G.; Baeza, C.; Angulo, C. Characterizing major avalanche episodes in space and time in the twentieth and early twenty-first centuries in the Catalan Pyrenees. *Cold Reg. Sci. Technol.* **2015**, *110*, 129–148. [CrossRef]
6. Furdada, G.; Margalef, A.; Trapero, L.; Pons, M.; Areny, F.; Baró, M.; Reyes, A.; Guinau, M. The Avalanche of Les Fonts d'Arinsal (Andorra): An Example of a Pure Powder, Dry Snow Avalanche. *Geosciences* **2020**, *10*, 126. [CrossRef]
7. Esteban, P.; Jones, P.D.; Martín-Vide, J.; Mases, M. Atmospheric circulation patterns related to heavy snowfall days in Andorra, Pyrenees. *Int. J. Clim.* **2005**, *25*, 319–329. [CrossRef]
8. Buisan, S.; López-Moreno, J.; Saz, M.; Kochendorfer, J. Impact of weather type variability on winter precipitation, temperature and annual snowpack in the Spanish Pyrenees. *Clim. Res.* **2016**, *69*, 79–92. [CrossRef]
9. Navarro-Serrano, F.; López-Moreno, J.I. Spatio-temporal analysis of snowfall events in the spanish Pyrenees and their relationship to atmospheric circulation. *Cuadernos Investig. Geográf.* **2017**, *43*, 233–254. [CrossRef]
10. Trapero, L.; Bech, J.; Lorente, J. Numerical modelling of heavy precipitation events over Eastern Pyrenees: Analysis of orographic effects. *Atmos. Res.* **2013**, *123*, 368–383. [CrossRef]
11. Trapero, L.; Bech, J.; Duffourg, F.; Esteban, P.; Lorente, J. Mesoscale numerical analysis of the historical November 1982 heavy precipitation event over Andorra (Eastern Pyrenees). *Nat. Hazards Earth Syst. Sci.* **2013**, *13*, 2969–2990. [CrossRef]
12. Vicente-Serrano, S.M.; Zabalza-Martínez, J.; Borràs, G.; López-Moreno, J.I.; Pla, E.; Pascual, D.; Savé, R.; Biel, C.; Funes, I.; Azorin-Molina, C.; et al. Extreme hydrological events and the influence of reservoirs in a highly regulated river basin of northeastern Spain. *J. Hydrol. Reg. Stud.* **2017**, *12*, 13–32. [CrossRef]
13. Madsen, H.; Lawrence, D.; Lang, M.; Martinkova, M.; Kjeldsen, T.R. Review of trend analysis and climate change projections of extreme precipitation and floods in Europe. *J. Hydrol.* **2014**, *519*, 3634–3650. [CrossRef]
14. Insua-Costa, D.; Lemus-Cánovas, M.; Miguez-Macho, G.; Llasat, M.C. Climatology and ranking of hazardous precipitation events in the western Mediterranean area. *Atmos. Res.* **2021**, *255*, 105521. [CrossRef]
15. Lemus-Canovas, M.; Lopez-Bustins, J.A.; Martin-Vide, J.; Royé, D. synoptReg: An R package for computing a synoptic climate classification and a spatial regionalization of environmental data. *Environ. Model. Softw.* **2019**, *118*, 114–119. [CrossRef]
16. Lagouvardos, K.; Dafis, S.; Giannaros, C.; Karagiannidis, A.; Kotroni, V. Investigating the Role of Extreme Synoptic Patterns and Complex Topography During Two Heavy Rainfall Events in Crete in February 2019. *Climate* **2020**, *8*, 87. [CrossRef]
17. Esteban, P.; Ninyerola, M.; Prohom, M. Spatial modelling of air temperature and precipitation for Andorra (Pyrenees) from daily circulation patterns. In *Proceedings of the Theoretical and Applied Climatology*; Springer: Wien, Austria, 2009; Volume 96, pp. 43–56.
18. Lemus-Canovas, M.; Lopez-Bustins, J.A.; Trapero, L.; Martin-Vide, J. Combining circulation weather types and daily precipitation modelling to derive climatic precipitation regions in the Pyrenees. *Atmos. Res.* **2019**, *220*, 181–193. [CrossRef]
19. Trigo, R.M.; DaCamara, C.C. Circulation weather types and their influence on the precipitation regime in Portugal. *Int. J. Clim.* **2000**, *20*, 1559–1581. [CrossRef]
20. Lorenzo, M.N.; Taboada, J.J.; Gimeno, L. Links between circulation weather types and teleconnection patterns and their influence on precipitation patterns in Galicia (NW Spain). *Int. J. Clim.* **2008**, *28*, 1493–1505. [CrossRef]
21. Cortesi, N.; Gonzalez-Hidalgo, J.C.; Trigo, R.M.; Ramos, A.M. Weather types and spatial variability of precipitation in the Iberian Peninsula. *Int. J. Clim.* **2014**, *34*, 2661–2677. [CrossRef]
22. Ramos, A.M.; Cortesi, N.; Trigo, R.M. Circulation weather types and spatial variability of daily precipitation in the Iberian Peninsula. *Front. Earth Sci.* **2014**, *2*, 25. [CrossRef]

23. Lemus-Canovas, M.; Ninyerola, M.; Lopez-Bustins, J.A.; Manguan, S.; Garcia-Sellés, C. A mixed application of an objective synoptic classification and spatial regression models for deriving winter precipitation regimes in the Eastern Pyrenees. *Int. J. Clim.* **2019**, *39*, 2244–2259. [CrossRef]
24. Jones, P.D.; Hulme, M.; Briffa, K.R. A comparison of Lamb circulation types with an objective classification scheme. *Int. J. Clim.* **1993**, *13*, 655–663. [CrossRef]
25. Carro-Calvo, L.; Ordóñez, C.; García-Herrera, R.; Schnell, J.L. Spatial clustering and meteorological drivers of summer ozone in Europe. *Atmos. Environ.* **2017**, *167*, 496–510. [CrossRef]
26. Martin-Vide, J.; Sanchez-Lorenzo, A.; Lopez-Bustins, J.A.; Cordobilla, M.J.; Garcia-Manuel, A.; Raso, J.M. Torrential rainfall in northeast of the Iberian Peninsula: Synoptic patterns and WeMO influence. *Adv. Sci. Res.* **2008**, *2*, 99–105. [CrossRef]
27. Lopez-Bustins, J.A.; Martin-Vide, J.; Sanchez-Lorenzo, A. Iberia winter rainfall trends based upon changes in teleconnection and circulation patterns. *Glob. Planet. Chang.* **2008**, *63*, 171–176. [CrossRef]
28. Sanchez-Lorenzo, A.; Calbó, J.; Martin-Vide, J.; Garcia-Manuel, A.; García-Soriano, G.; Beck, C. Winter "weekend effect" in southern Europe and its connections with periodicities in atmospheric dynamics. *Geophys. Res. Lett.* **2008**, *35*, L15711. [CrossRef]
29. Nishiyama, K.; Endo, S.; Jinno, K.; Bertacchi Uvo, C.; Olsson, J.; Berndtsson, R. Identification of typical synoptic patterns causing heavy rainfall in the rainy season in Japan by a Self-Organizing Map. *Atmos. Res.* **2007**, *83*, 185–200. [CrossRef]
30. Meseguer-Ruiz, O.; Ponce-Philimon, P.I.; Baltazar, A.; Guijarro, J.A.; Serrano-Notivoli, R.; Olcina Cantos, J.; Martin-Vide, J.; Sarricolea, P. Synoptic attributions of extreme precipitation in the Atacama Desert (Chile). *Clim. Dyn.* **2020**, *55*, 3431–3444. [CrossRef]
31. Kunkel, K.E.; Stevens, S.E.; Stevens, L.E.; Karl, T.R. Observed Climatological Relationships of Extreme Daily Precipitation Events With Precipitable Water and Vertical Velocity in the Contiguous United States. *Geophys. Res. Lett.* **2020**, *47*, e2019GL086721. [CrossRef]
32. Sillmann, J.; Kharin, V.V.; Zwiers, F.W.; Zhang, X.; Bronaugh, D. Climate extremes indices in the CMIP5 multimodel ensemble: Part 2. Future climate projections. *J. Geophys. Res. Atmos.* **2013**, *118*, 2473–2493. [CrossRef]
33. Cuadrat, J.M.; Serrano-Notivoli, R.; Tejedor, E.; Saz, M.Á.; Prohom, M.; Cunillera, J.; Llabrés, A.; Trapero, L.; Pons, M.; López-Moreno, J.I.; et al. CLIMPY: Climate of the Pyrenees. *Zenodo* **2020**. [CrossRef]
34. Serrano-Notivoli, R.; Beguería, S.; Saz, M.Á.; Longares, L.A.; De Luis, M. SPREAD: A high-resolution daily gridded precipitation dataset for Spain—An extreme events frequency and intensity overview. *Earth Syst. Sci. Data* **2017**, *9*, 721–738. [CrossRef]
35. Hersbach, H.; Bell, B.; Berrisford, P.; Hirahara, S.; Horányi, A.; Muñoz-Sabater, J.; Nicolas, J.; Peubey, C.; Radu, R.; Schepers, D.; et al. The ERA5 global reanalysis. *Q. J. R. Meteorol. Soc.* **2020**, *146*, 1999–2049. [CrossRef]
36. Stein, A.F.; Draxler, R.R.; Rolph, G.D.; Stunder, B.J.B.; Cohen, M.D.; Ngan, F. Noaa's hysplit atmospheric transport and dispersion modeling system. *Bull. Am. Meteorol. Soc.* **2015**, *96*, 2059–2077. [CrossRef]
37. Kalnay, E.; Kanamitsu, M.; Kistler, R.; Collins, W.; Deaven, D.; Gandin, L.; Iredell, M.; Saha, S.; White, G.; Woollen, J.; et al. The NCEP/NCAR 40-Year Reanalysis Project. *Bull. Am. Meteorol. Soc.* **1996**, *77*, 437–472. [CrossRef]
38. Martin-Vide, J.; Lopez-Bustins, J.-A. The Western Mediterranean Oscillation and rainfall in the Iberian Peninsula. *Int. J. Clim.* **2006**, *26*, 1455–1475. [CrossRef]
39. Conte, M.; Giuffrida, A.; Tedesco, S. Mediterranean Oscillation: Impact on Precipitation and Hydrology in Italy. *Conf. Clim. Water* **1989**, *9*, 121–137.
40. Redolat, D.; Monjo, R.; Lopez-Bustins, J.A.; Martin-Vide, J. Upper-Level Mediterranean Oscillation index and seasonal variability of rainfall and temperature. *Theor. Appl. Clim.* **2019**, *135*, 1059–1077. [CrossRef]
41. Hurrell, J.W. Decadal trends in the North Atlantic oscillation: Regional temperatures and precipitation. *Science* **1995**, *269*, 676–679. [CrossRef]
42. Llasat, M.-C. An objective classification of rainfall events on the basis of their convective features: Application to rainfall intensity in the northeast of Spain. *Int. J. Clim.* **2001**, *21*, 1385–1400. [CrossRef]
43. Lopez-Bustins, J.; Arbiol-Roca, L.; Martin-Vide, J.; Barrera-Escoda, A.; Prohom, M. Intra-annual variability of the Western Mediterranean Oscillation (WeMO) and occurrence of extreme torrential precipitation in Catalonia (NE Iberia). *Nat. Hazards Earth Syst. Sci.* **2020**, *20*, 2483–2501. [CrossRef]
44. De Luis, M.; González-Hidalgo, J.C.; Raventós, J. Effects of fire and torrential rainfall on erosion in a Mediterranean gorse community. *Land Degrad. Dev.* **2003**, *14*, 203–213. [CrossRef]
45. Cattell, R.B. The scree test for the number of factors. *Multivar. Behav. Res.* **1966**. [CrossRef]
46. Richman, M.B. Rotation of principal components. *J. Clim.* **1986**, *6*, 293–335. [CrossRef]
47. Lavers, D.A.; Villarini, G.; Allan, R.P.; Wood, E.F.; Wade, A.J. The detection of atmospheric rivers in atmospheric reanalyses and their links to British winter floods and the large-scale climatic circulation. *J. Geophys. Res. Atmos.* **2012**, *117*, 117. [CrossRef]
48. Gustafsson, M.; Rayner, D.; Chen, D. Extreme rainfall events in southern Sweden: Where does the moisture come from? *Tellus A Dyn. Meteorol. Oceanogr.* **2010**, *62*, 605–616. [CrossRef]
49. Fleming, Z.L.; Monks, P.S.; Manning, A.J. Review: Untangling the influence of air-mass history in interpreting observed atmospheric composition. *Atmos. Res.* **2012**, *104–105*, 1–39. [CrossRef]
50. Martin-Vide, J. Spatial distribution of a daily precipitation concentration index in peninsular Spain. *Int. J. Clim.* **2004**, *24*, 959–971. [CrossRef]

51. Lopez-Bustins, J.A.; Lemus-Canovas, M. The influence of the Western Mediterranean Oscillation upon the spatio-temporal variability of precipitation over Catalonia (northeastern of the Iberian Peninsula). *Atmos. Res.* **2020**, *236*, 104819. [CrossRef]
52. de Luis, M.; Brunetti, M.; Gonzalez-Hidalgo, J.C.; Longares, L.A.; Martin-Vide, J. Changes in seasonal precipitation in the Iberian Peninsula during 1946-2005. *Glob. Planet. Chang.* **2010**, *74*, 27–33. [CrossRef]
53. Merino, A.; Fernández-Vaquero, M.; López, L.; Fernández-González, S.; Hermida, L.; Sánchez, J.L.; García-Ortega, E.; Gascón, E. Large-scale patterns of daily precipitation extremes on the Iberian Peninsula. *Int. J. Clim.* **2016**, *36*, 3873–3891. [CrossRef]
54. Pérez-Zanón, N.; Casas-Castillo, M.C.; Peña, J.C.; Aran, M.; Rodríguez-Solà, R.; Redaño, A.; Solé, G. Analysis of synoptic patterns in relationship with severe rainfall events in the Ebre Observatory (Catalonia). *Acta Geophys.* **2018**, *66*, 405–414. [CrossRef]
55. Bonsoms, J.; Gonzalez, S.; Prohom, M.; Esteban, P.; Salvador-Franch, F.; López-Moreno, J.I.; Oliva, M. Spatio-temporal patterns of snow in the Catalan Pyrenees (NE Iberia). *Int. J. Clim.* **2021**. Under review. [CrossRef]
56. Insua-Costa, D.; Miguez-Macho, G.; Llasat, C. Local and remote moisture sources for extreme precipitation: A study of the two catastrophic 1982 western Mediterranean episodes. *Hydrol. Earth Syst. Sci.* **2019**, *23*, 3885–3900. [CrossRef]
57. Pineda, N.; Esteban, P.; Trapero, L.; Soler, X.; Beck, C. Circulation types related to lightning activity over Catalonia and the Principality of Andorra. *Phys. Chem. Earth* **2010**, *35*, 469–476. [CrossRef]
58. Martinez-Artigas, J.; Lemus-Canovas, M.; Lopez-Bustins, J.A. Precipitation in peninsular Spain: Influence of teleconnection indices and spatial regionalisation. *Int. J. Clim.* **2021**, *41*, E1320–E1335. [CrossRef]
59. Rodó, X.; Baert, E.; Comin, F.A. Variations in seasonal rainfall in Southern Europe during the present century: Relationships with the North Atlantic Oscillation and the El Niño-Southern Oscillation. *Clim. Dyn.* **1997**, *13*, 275–284. [CrossRef]
60. Esteban, P.; Soler, X.; Prohom, M.; Planchon, O. *La Distribución de la Precipitación a Través del Índice NAO. El Efecto del Relieve a Escala Local: El Pirineo Oriental*; Publicaciones de la Sociedad Española de Climatología: Palma de Mallorca, Spain, 2002; pp. 25–34.
61. Pastor, F.; Valiente, J.A.; Estrela, M.J. Sea surface temperature and torrential rains in the Valencia region: Modelling the role of recharge areas. *Hazards Earth Syst. Sci.* **2015**, *15*, 1677–1693. [CrossRef]